6

Climatology of the U.S. Inter-Mountain West

S. Y. Simon Wang and Robert R. Gillies
Utah Climate Center / Department of Plants, Soil and Climate
Utah State University, Logan UT
USA

1. Introduction

The Inter-Mountain West (IMW) of North America is a region that lies between the Rocky Mountains to the east and the Cascades and Sierra Nevada to the west (**Fig. 1**). The climate of the IMW is generally semi-arid but this varies by location and elevation. An estimated 50-80% of the IMW's streams and rivers are fed by mountain snowpack (Marks and Winstral 2001), while the majority of the streams and rivers flow into desert sinks or closed-basin lakes such as the Great Salt Lake (**Fig. 1**). These streams and rivers create some agriculturally productive areas in the otherwise dry basins and mountain valleys. In particular, the Colorado River supplies water to the population-booming southwestern

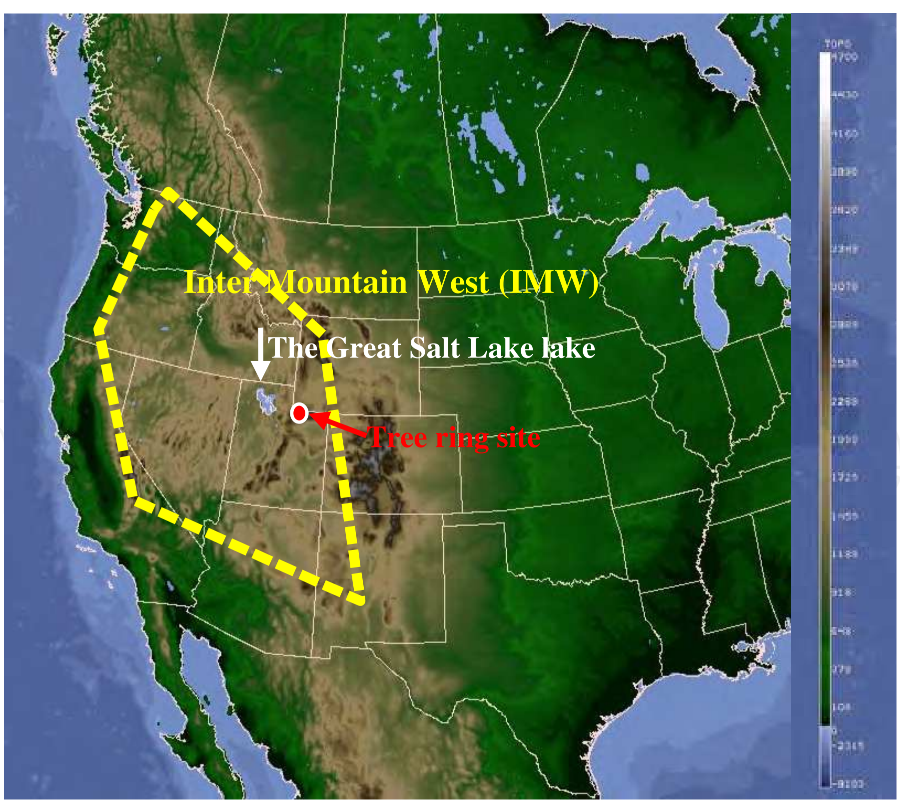

Fig. 1. The Inter-Mountain West (IMW) region (yellow dashed outline), the Great Salt Lake (arrow), and the tree ring site for the reconstructed precipitation (red dot) as shown in Fig. 2. Background is terrain (map source: Unidata).

states and cities. Climate in the Colorado River Basin has been a subject of intense research due to its projected drying trend (Barnett and Pierce 2008). Change in winter precipitation regime (i.e. ratio between rainfall and snowfall) is also a subject of interest not only because its role in water resource but also its impact on recreational (ski) industry in the IMW.

Paleoclimate records indicate that the current mean state of climate in the IMW may not be stable. Over most of the past millennium, droughts in the IMW were generally more intense and lasted longer than those experienced in the 20th century, which had included the "severe droughts" of the 1930s and 1950s. **Fig. 2** presents a long-term precipitation proxy based on tree ring data collected near the upstream Colorado River in northeastern Utah (red dot in Fig. 1). It is immediately apparent that even the worst droughts of the 20th century are dwarfed in both magnitude and duration compared to the previous droughts of the 14th-18th centuries, as well as the megadrought of the 13th century (Gray et al. 2004). Moreover, the 20th century has been a relatively wet period when compared to the pre-19th century era. These observations may imply an unstable state of modern-time, relatively wet precipitation regime that carries the potential to resume its pre-18th century climatology with longer, deeper droughts. Previous studies of tree ring-based drought analysis (Cook et al. 1997; Herweijer et al. 2007) have found a similar non-stationarity in the IMW climate change, in the sense that drought frequency has shifted from being centennial and more intense in the early millennium into being multi-decadal and less intense in the later millennium. To what extent such a cyclic feature may change or persist into the future is important information for water management.

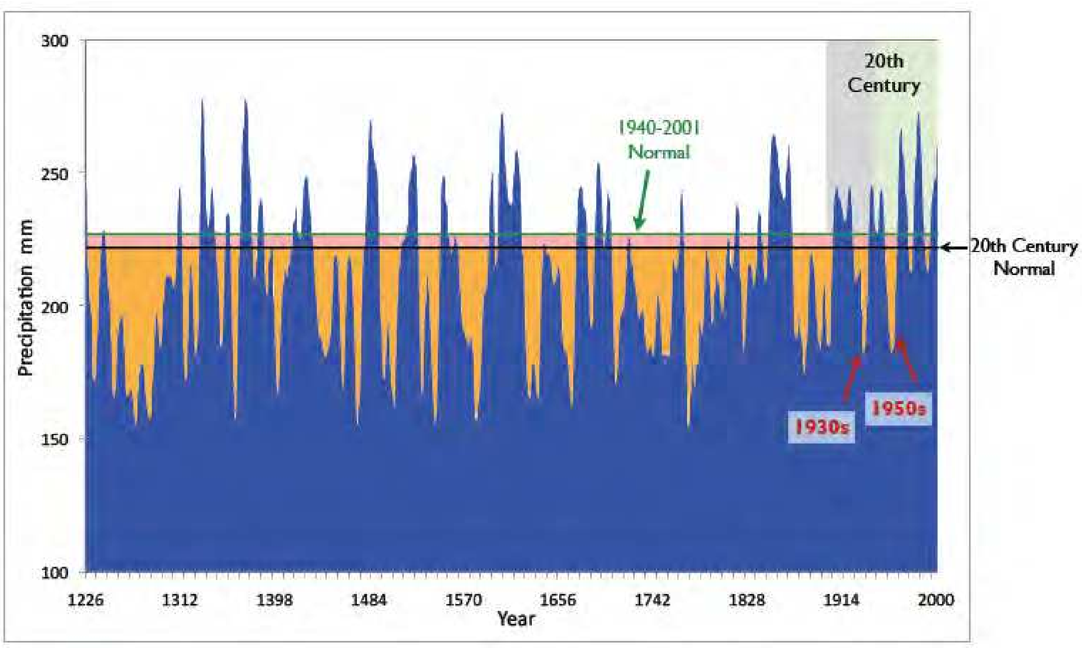

Fig. 2. (a) Tree ring-reconstructed annual precipitation proxy (blue shadings) generated from samples collected in northeastern Utah (red dot in Fig. 1) by Gray et al. (2004). Orange shadings indicate precipitation deficits under the 1940-2001 mean.

It is now well established that quasi-periodic climate modes in the Pacific and Atlantic Oceans modulate the IMW climate. A sizable body of research (Barlow et al. 2001; Schubert et al. 2004, 2009; Seager et al. 2005; among others) has explored the physical linkage between the Pacific sea surface temperature (SST) variations and climate anomalies in North America. Such Pacific SST variations include *(a)* multi-decadal modes like the Pacific Decadal Oscillation (PDO) (Mantua et al. 1997) and the Interdecadal Pacific Oscillation (IPO; Folland et al. 2002), *(b)* decadal modes such as the Pacific quasi-decadal oscillation (QDO) (Tourre et al. 2001; White et al. 2003), and *(c)* interannual modes associated with the El Niño-Southern Oscillation (ENSO). Covariability between these Pacific climate modes and the drought evolution in the IMW has also been reported (e.g., Sangoyomi 1993; Zhang and Mann 2005). Moreover, the IMW's climate regime is further complicated by unique seasonal variations in precipitation, characterized by a combination of annual and semiannual cycles whose timing varies across the region. Such a complex climatology poses a great challenge to climate models and climate prediction.

This chapter discusses the complex climate regimes of the IMW with a focus on four different timescales: (Section 2) seasonal and intraseasonal, section (3) interannual, and section (4) decadal variabilities. These different scales of climate variability interact with each other and this further modulates the IMW climate variability; Section 5 discusses such an interaction. Simulations of the IMW climate by some global and regional climate models are evaluated. Finally, Section 6 provides a summary of the chapter.

2. Seasonal climate variability

a. Annual and semiannual cycles

Pronounced annual and semiannual cycles in precipitation characterize the IMW's climatology. Earlier studies (e.g., Hsu and Wallace 1976) have noted that the phase of the annual cycle changes by six months going from east to west across the Rocky Mountains, while the semiannual cycle changes phase from north to south. The precipitation patterns corresponding to these annual and semiannual cycles are illustrated in **Figs. 3a** and **3b**, respectively, through correlation maps of the first and second principal components (PC) of monthly data of the Climate Prediction Center Merged Analysis of Precipitation (CMAP; Xie and Arkin 1997). In the IMW, the combination of the annual cycle (i.e. east-west) and semiannual cycle (i.e. north-south) forms four seasonal precipitation regimes that meet in the central IMW near Utah. However, atmospheric general circulation models (AGCMs) do not simulate well such seasonal cycles in precipitation, particularly the semiannual cycle (Boyle 1998). In addition, complexity also arises from interaction between the atmospheric circulation and orography encountered in the IMW, amplifying such model deficiencies. For instance, the NCAR Community Climate Model version 3 (CCM3) produced a distorted semiannual precipitation pattern in the IMW, shown in **Fig. 3c**. Wang et al. (2009a) have suggested that the semiannual precipitation cycle in the IMW is likely related to the onset and development of the North American Monsoon (NAM) that features a change in the upper-level circulation regime, evolving from a large-scale trough in spring into a quasi-stationary anticyclone in the monsoon months (Higgins et al. 1997). The circulation regime change is followed by a precipitation phase reversal in the north-south direction, as is shown in **Fig. 3b**. A similar but weaker change in circulation pattern occurs in early spring, when an upper-level trough forms over the southwest U.S. and gradually migrates westward (Wang and Chen 2009). These features pose a great challenge to AGCMs in simulating the precipitation seasonal cycle of the IMW.

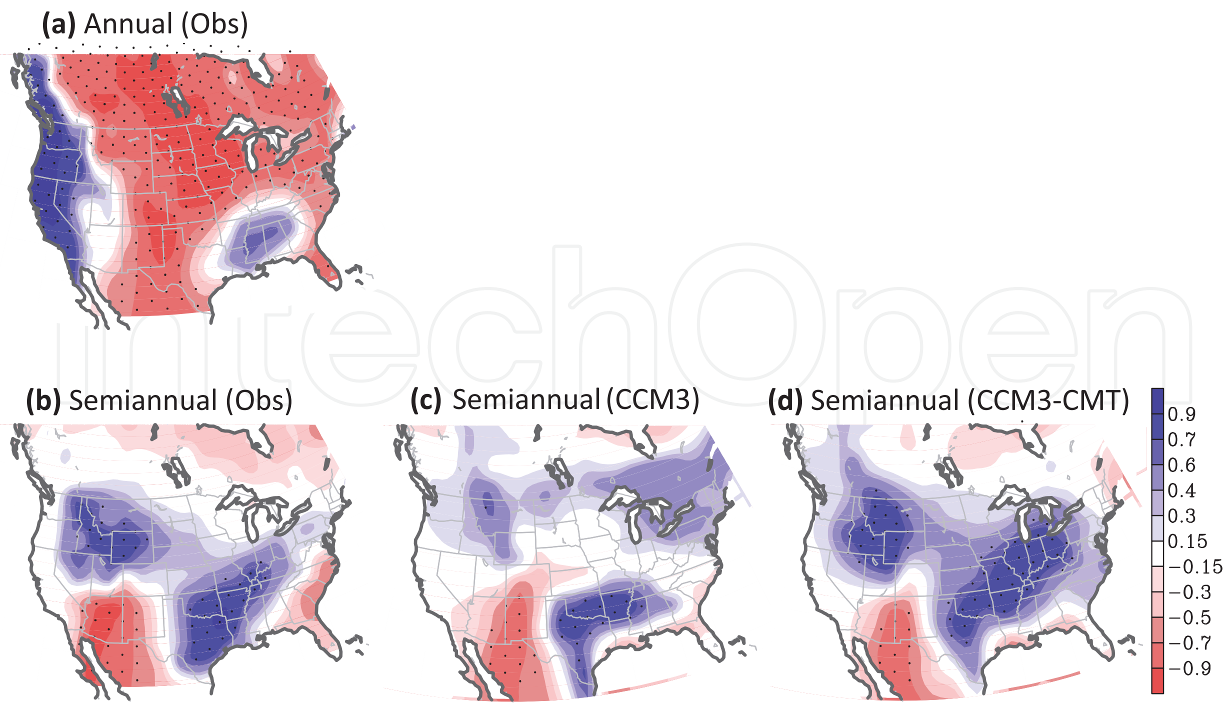

Fig. 3. Correlation maps of monthly precipitation anomalies with respect to (a) the annual cycle and (b) the semiannual cycle using the CMAP (observed) data. (c) and (d) Same as (b) but using the control run and the coupled-CMT run of CCM3, respectively. The CCM3 precipitation was correlated with the PC time series of the CMAP (observed) data.

To further examine the AGCM performance, we adopted a set of CCM3 simulations with (a) the control run as in **Fig. 3c** and (b) the inclusion of a convective momentum transport (CMT) in the convection scheme as in **Fig. 3d**, generated by Wu et al. (2007). The reason here to include the CMT experiment was to evaluate the impact of convective processes on the simulated seasonal cycles, since the semiannual cycle of the IMW precipitation is linked to the NAM onset – i.e. convective rainfall. In AGCMs, CMT is far more intricate to parameterize than thermodynamic transports due to complicated cloud-scale pressure gradients induced by organized convection (Moncrieff 1992; Wu et al. 2007). As shown in **Fig. 3d**, the inclusion of CMT considerably improves the simulation of the semiannual precipitation change. Of note is that the improvement appears not only in the IMW but also in the central and southeast United States. An improvement like this signifies that the semiannual cycle in precipitation is closely related to cloud system feedback, since convective clouds not only release latent heat and redistribute heat/moisture but also transport momentum. Possibly, the convective momentum tendencies adjust the local Hadley circulation across the IMW, while the responses of meridional wind to the more realistic heating improve the secondary meridional circulation associated with the NAM development.

Regional climate models (RCMs) are thought to produce a more realistic precipitation seasonal cycle than AGCMs, particularly in regions having topographically enhanced precipitation (Leung et al. 2006). The IMW's geography is characterized by four major mountain ranges: 1) the Cascade Range, 2) the Bitterroot Range, 3) the Wasatch Range and 4) the Colorado Rockies, denoted in **Fig. 4a** as regions 1-4, while central Arizona is denoted as region 5. In the cold season, precipitation occurs mainly on the windward side of these mountain ranges (**Fig. 4b**).

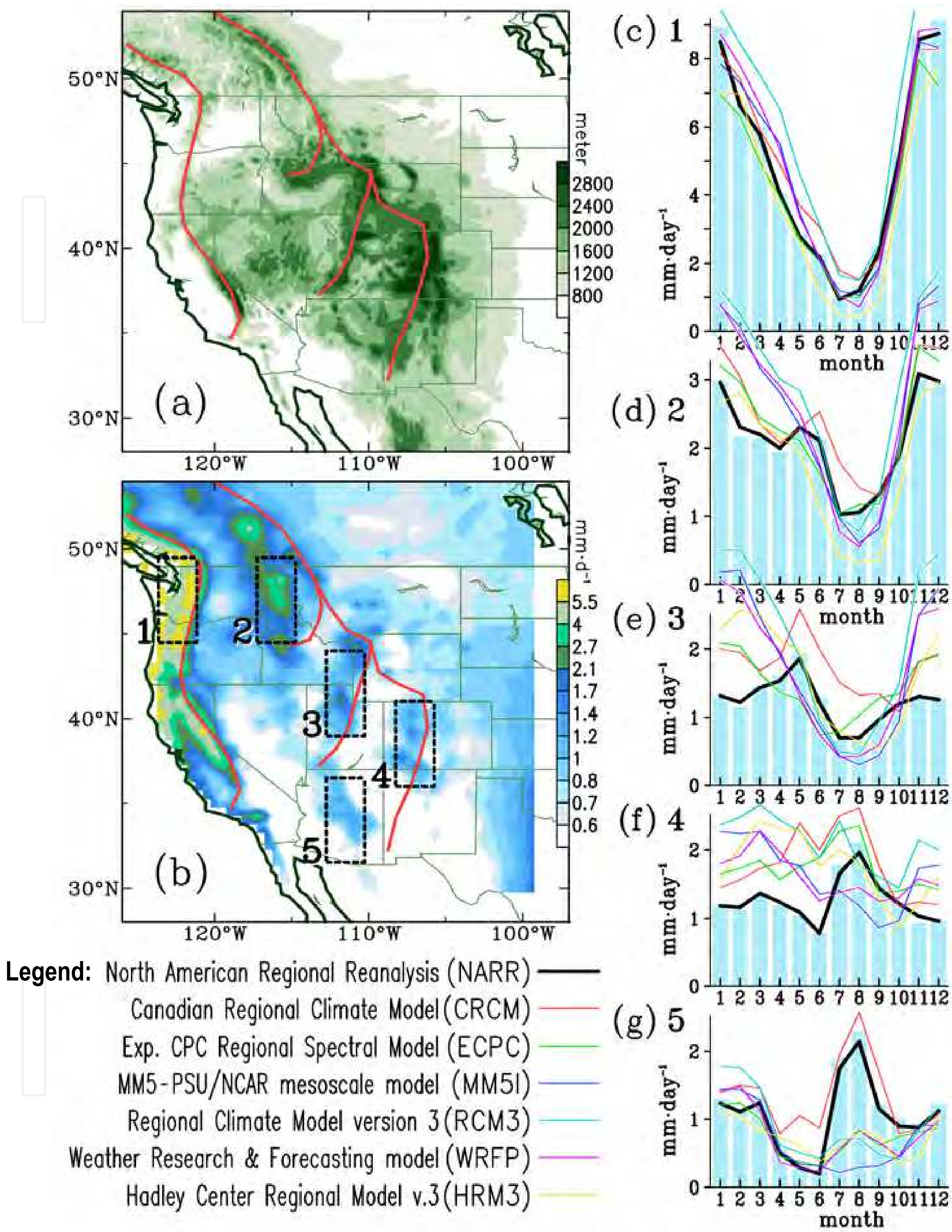

Fig. 4. (Adopted from Wang et al. 2009a) (a) Orography and (b) cold-season rainfall (November-May, UDel) of the IMW, where the red lines outline the major mountain ranges. (c)-(g) Monthly histograms of UDel rainfall averaged from the five regions indicated in (b), superimposed with the corresponding precipitation of NARR (thick black line) and all RCMs (color lines). The abbreviation of the RCMs and their corresponding color codes are given under (b). Note the precipitation scale in (c) is twice of that in (d)-(g).

Wang et al. (2009a) showed that, from the coastal area toward the IMW (i.e. regions 1 through 4) the seasonal cycle evolves from a winter regime toward the summer regime with increasing semiannual variability. This transition of the precipitation seasonal cycle is illustrated in **Figs. 4c-g** by two sets of observation – the North American Regional Reanalysis (NARR) (Mesinger et al. 2006; black line) and the University of Delaware (UDel) (Legates and Willmott 1990; blue bar). Apparently, spring precipitation becomes important in region 2 and peaks in region 3, but then decreases in regions 4 and 5 where a monsoon rainfall regime prevails in summer, corresponding to the combination of the annual and semiannual cycles.

Analyzing the precipitation climatology simulated by six RCMs participating in the North American Regional Climate Change Assessment Program (NARCCAP; Mearns et al. 2009), in which the RCMs were driven by the same boundary conditions of a global reanalysis, Wang et al. (2009a) found that the RCMs have a difficulty in replicating the precipitation seasonal cycle. As revealed in **Figs. 4c-g**, in the Cascade Range (region 1) where the annual cycle is dominant, the phases of the RCM precipitation show marked consistency with the observations. However, beginning in region 2, the RCM precipitation variation increasingly departs from the observation and the simulated winter precipitation amounts are consistently too large. In the inner IMW (region 3), where the annual cycle is weak, four out of the six RCMs still produce a dominant annual cycle and do not capture the elevated spring precipitation. In region 4 where winter precipitation and summer monsoon rains have equal contributions, the RCMs generate mixed signals that disagree with the observations. In region 5, the simulated monsoon precipitation is only captured by one model (red line), which used spectral nudging (i.e., incorporating reanalysis information into the simulation domain). In summary, the performances of the RCMs are weakest in the inner IMW (i.e. regions 2-4) in which the transition of seasonal climate regimes takes place. Due to the overprediction in winter precipitation, most RCMs have a tendency to produce too strong of an annual cycle and this obscures the relatively good performance in the semiannual cycle (Wang et al. 2009a). Such a character differs from most AGCMs that do not simulate the semiannual cycle well. The overprediction of winter precipitation also affects the simulated ENSO impact on the IMW climate; this model deficiency will be further discussed in Section 3.

b. Intraseasonal variation

Winter and spring weather conditions in the IMW are characterized by considerable intraseasonal variations (on the order of 3-8 weeks). These intraseasonal variations are linked to (1) the evolution of free external Rossby waves (Lau and Nath 1999), (2) tropical-midlatitude interaction associated with the Madden-Julian Oscillation (MJO) (Mo 1999), and (3) short Rossby waves propagating through the jet stream waveguide, referred to as the circumglobal teleconnection (CGT) (Branstator 2002). For external Rossby waves, the forcing and dynamics have been studied extensively; i.e. the waves slowly propagate westward in response to the planetary β effect at a speed coincident with the intraseasonal timescale (Branstator 1987; Horel and Mechoso 1988; Lau and Nath 1999). On the other hand, the midlatitude response of the circulation to the tropical MJO forcing normally results in stationary or eastward-moving synoptic-scale waves (Mo and Paegle 2005). For the CGT, upstream transient vorticity forcing, usually occurring in Eurasia and East Asia, produces short-wave response with the energy propagating eastward towards

North America. The CGT pattern is known to change month-by-month (i.e. intraseasonal) (Ding and Wang 2005), yet it has a profound impact on extreme spring weather conditions in the IMW (Wang et al. 2010b).

A recent study (Gillies et al. 2010a) has shown that winter weather – including temperature, precipitation and snowpack – fluctuates in strong association with a "30-day mode" that dominates persistent weather regimes in the IMW. Analyzing the geopotential height sounding data in Salt Lake City during 1980-2008, Gillies et al. (2010a) constructed a composite lifecycle of the 30-day mode (**Fig. 5a**). This 30-day mode strongly affects precipitation and snow depth over the IMW (**Fig. 5b**; centered in Salt Lake City with a 200 km radius), as well as temperature that effects snowmelt. Based on the 8-phase lifecycle of the 30-day mode, Gillies et al. (2010b) constructed the composite patterns of the 200-mb streamfunction and velocity potential (**Fig. 6**). The composite lifecycle of the 30-day mode – i.e. centered in the IMW – depicts a global eastward propagation of the velocity potential with a predominant zonal wave-1 pattern, which resembles the signature MJO structure. Meanwhile, a series of short-wave cells is excited within the eastward propagating velocity potential and propagates towards North America. At phases 2-3 when a stationary ridge prevails over the Great Basin, the associated wave train follows the "great circle" route of the Pacific-North America (PNA) pattern (Horel and Wallace 1981). An oppositely signed circulation anomaly appears at phases 6-7. Despite the propagating feature in the velocity potential, the streamfunction wave trains appear to be quasi-stationary. Such a feature underscores the fact that wintertime stationary waves in North America (and in the IMW) fluctuate in response to the tropical–extratropical linkages of the MJO (e.g., Kushnir 1987; Mo and Paegle 2005). These results indicate that the occurrences of either persistent ridging events or prolonged precipitation spells in the IMW are "phase locked" with the MJO evolution – at least at the higher-frequency end of the MJO spectrum that spans 30-60 days.

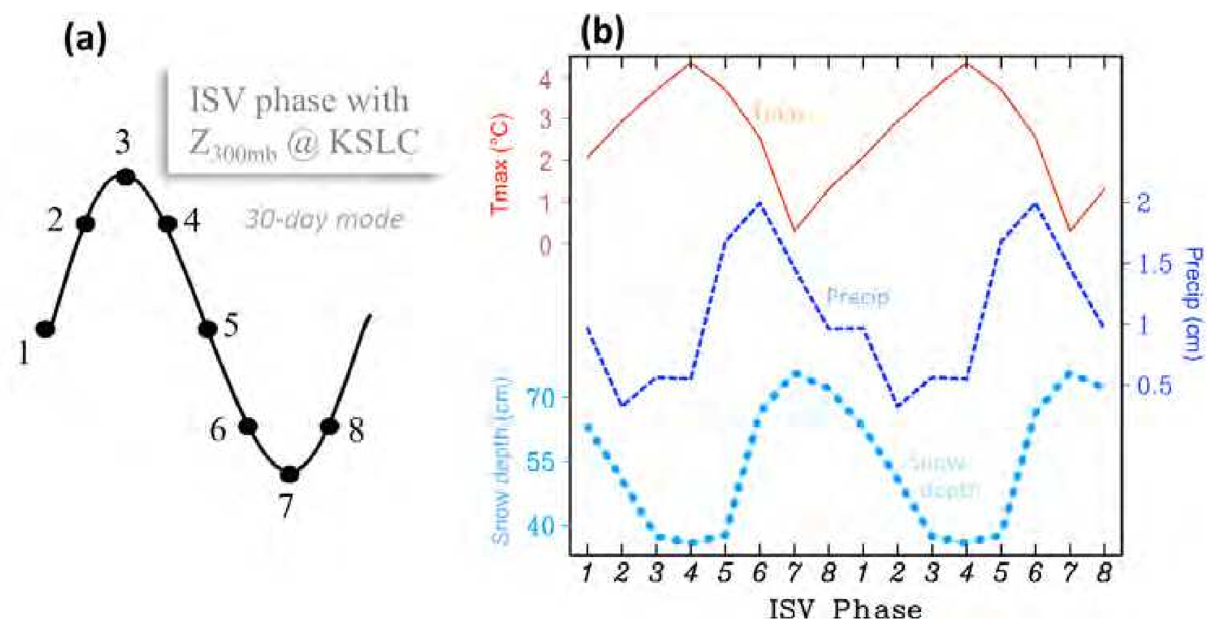

Fig. 5. (a) Lifecycle of the intraseasonal variability (ISV) based on Salt Lake City sounding of geopotential height (300mb), and (b) the 8-phase composites of Tmax (red), precipitation (blue dashed), and snow depth (cyan dotted) in Utah and upper Colorado Basin during 1980-2008 (after *Gillies et al. 2010a*).

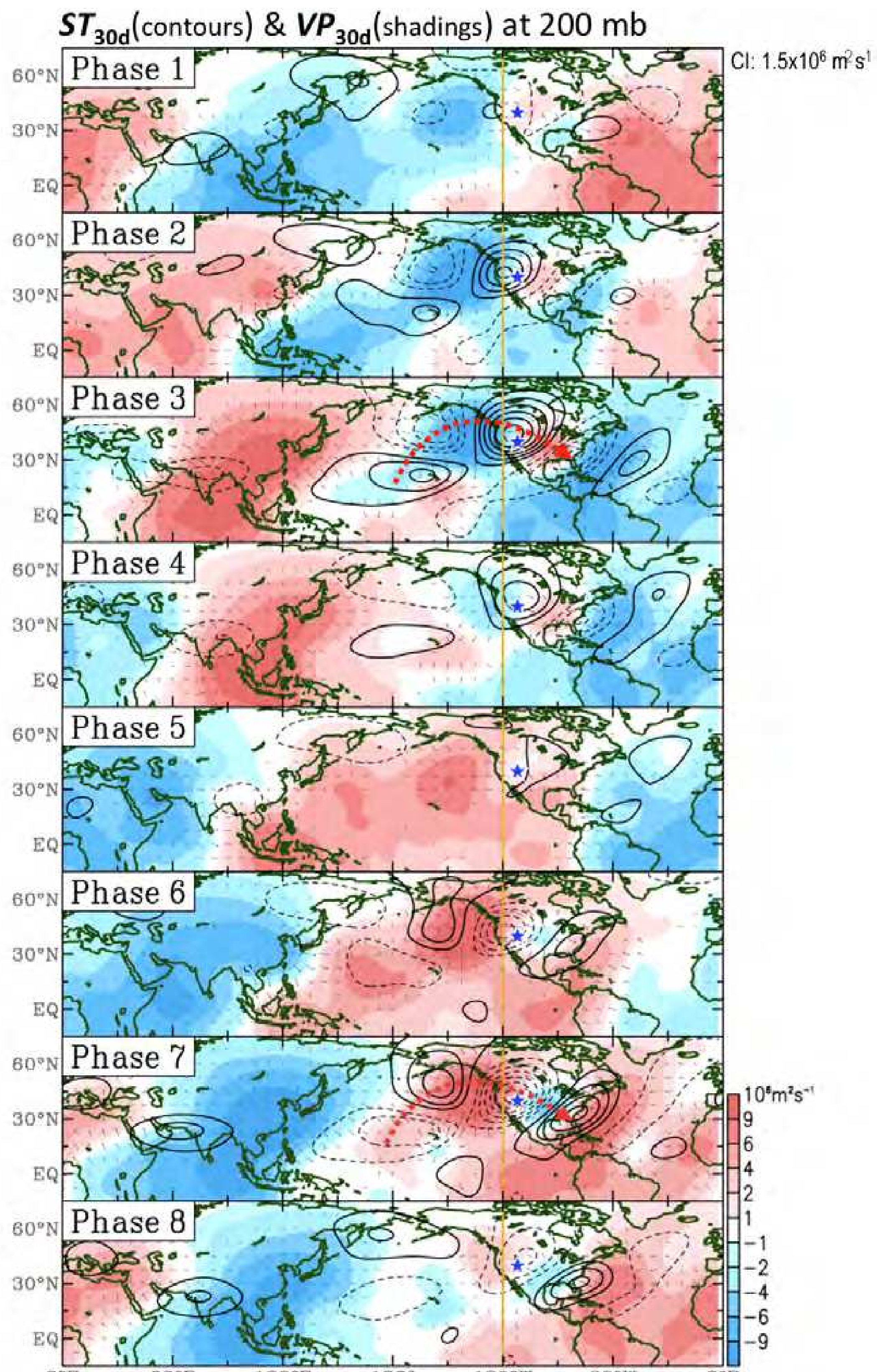

Fig. 6. Eight-phase composites of the 200mb velocity potential (shadings) and streamfunction constructed form the 30-day mode at Salt Lake City. Adopted from *Gillies et al. (2010b)* with permission from the American Meteorological Society.

3. Interannual variability

The impact of ENSO on precipitation and drought anomalies over western North America has been studied extensively. It is now well established that ENSO tends to produce a so-called North American dipole structure in precipitation and temperature, encompassing the Pacific Northwest and the Southwest with opposite polarity (Dettinger et al. 1998; and subsequent works). However, short-term climate forecasts (6 months to 2 years) based on this conceptual model have frequently failed during the recent decade (Wood 2011). Past studies (Rajagopalan and Lall 1998; Zhang and Mann 2005) have noted that the central part of the IMW is shielded from direct influence of ENSO as the region lies between the marginal zone of the north-south dipole pattern. Later studies (Hidalgo and Dracup 2003; Brown 2011) also found that the ENSO-climate connection in the IMW is not stable; rather, it fluctuates following a long-term oscillatory manner. This feature is further discussed in Section 5.

The CGT pattern (cf. Section 2b), which is characterized as a short Rossby wave train along the jet stream waveguide with a zonal wave-5 structure (Branstator 2002; Ding and Wang 2005), has been found to be linked to persistent rainy conditions over the IMW (Wang et al. 2010b). The spatial scale of the CGT wave train is shorter than that of the classic PNA pattern (wave 1-3; Hoskins and Karoly 1981), while its variability is *uncorrelated* with ENSO (Ding and Wang 2005). During spring, the North American circulations undergo a considerable change as the jet stream shifts rapidly northward. From April to July, a synoptic-scale trough develops over the southwest U.S., deepens and migrates to the West Coast and eventually merges with the oceanic trough over the North Pacific (Higgins et al. 1997; Wang and Chen 2009). The development of this trough enhances moisture and facilitates synoptic disturbances toward the IMW during spring, contributing to the rainy season there (cf. Fig. 4e).

Such a seasonal transition takes place through the formation of a standing wave train, manifest as stationary short waves embedded in the climatological jet stream (**Fig. 7a**). The distinct short-wave trough over the West Coast (arrow indicated) reflects the spring trough that enhances precipitation in the IMW. Wang et al. (2010b) found that extremely wet spring seasons in the IMW often occur with the presence of the CGT. Specifically, a *wet* (dry) spring in the IMW occurs when the CGT is *in-phase* (out-of-phase) with the standing wave train. For example, **Fig. 7b** shows the record precipitation that occurred in June 2009 as the climatological trough considerably deepened and was embedded in a series of short waves. Here, the CGT is further illustrated by the filtered geopotential height in the zonal wave-5 regime using harmonic analysis. Visual comparison between **Figs. 7a** and **7b** indicates that the 2009 wave train is in-phase with the standing wave train. Analyzing a 50-year period of two reanalysis datasets (NCEP and ERA; see caption) through the empirical orthogonal function (EOF) analysis, Wang et al. (2010b) confirmed the CGT linkage with the spring precipitation anomalies in the IMW. As shown in **Fig. 7c**, the first leading mode (26%) depicts the CGT as an amplification effect of the standing wave train (due to their coincident phases). Comparison of the EOF time series with the IMW precipitation anomalies in **Fig. 7d** further reveals that precipitation anomalies were clearly dependent with the phasing of the CGT.

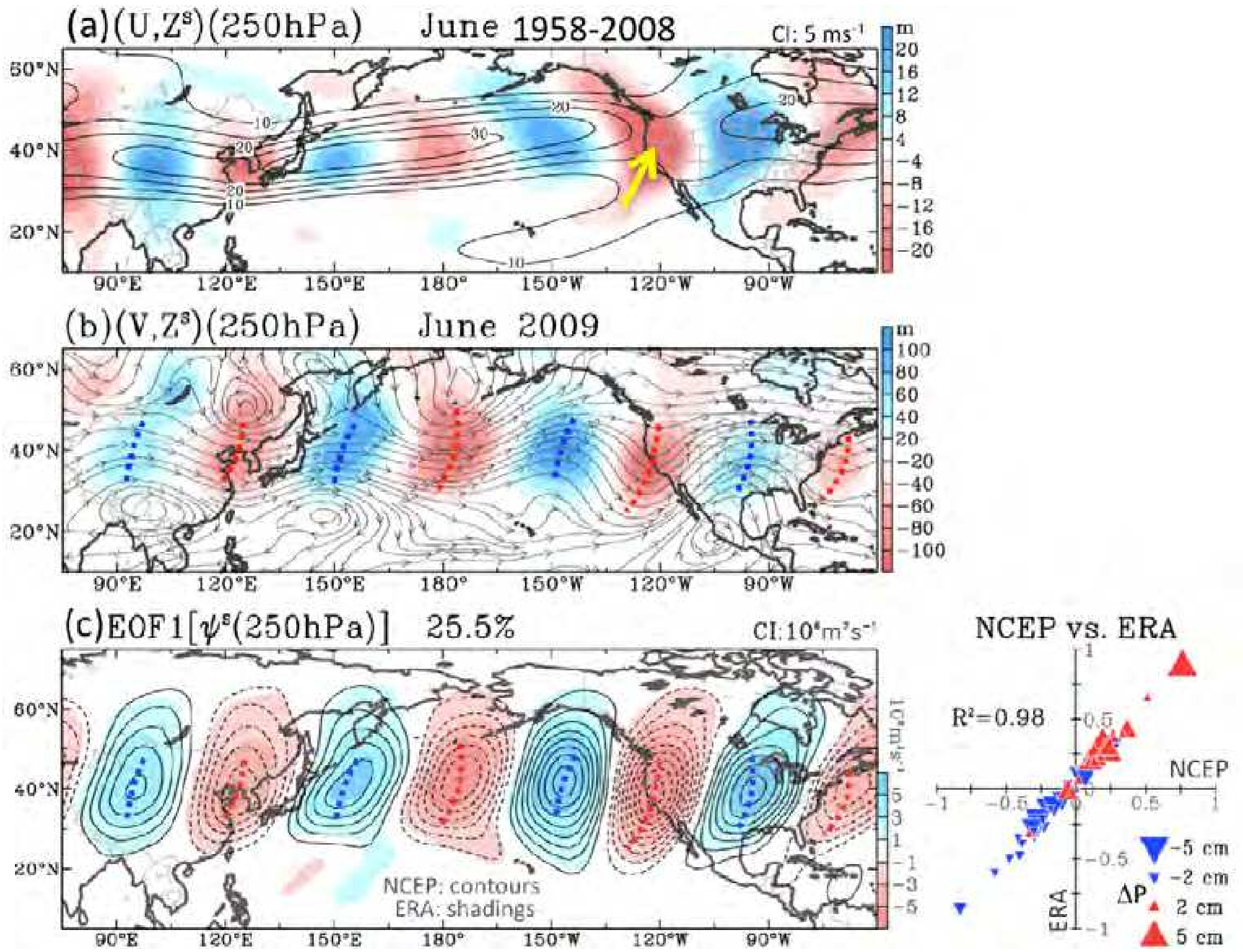

Fig. 7. (a) long-term 250hPa zonal wind (contours) and the shortwave-regime geopotential height (shadings; zonal wave-5) in June; yellow arrow indicates the spring trough. (b) The 250hPa streamlines and shortwave-regime geopotential height (shadings) in June 2009, marked with trough (red) and ridge (blue) lines. Note the consistent phases of geopotential height between (a) and (b). (c) First EOF of shortwave-regime streamfunction at 250 hPa from two reanalyses: NCEP (contours; Kalnay et al. 1996) and ERA (shadings, combined from ERA40 and ERA-Interim; Simmons et al. 2007). (d) Relationship between the first EOFs of NCEP1 and ERA, with the scatters represented by the IMW precipitation anomalies (ΔP; Legates and Willmott 1990) in terms of sign and size (After Wang et al. 2010b).

As mentioned in Section 2, Wang et al. (2009a) found that precipitation simulations by the NARCCAP RCMs (Section 2a) exhibit a “false” ENSO signal in the central IMW, likely due to their general tendency to overpredict winter precipitation. By examining the ENSO precipitation pattern constructed from the composite differences between six El Niño (1982/83, 87/88, 91/92, 94/95, 97/98, 2002/03) and four La Niña (1984/85, 88/89, 95/96, 98-2001) winters, which was based on the NOAA Climate Prediction Center[1], **Fig. 8a** reveales the typical north-south precipitation dipole over the western United States. This precipitation dipole is reasonably simulated by the NARCCAP models. However, in the central IMW (i.e. regions 3 and 4 in Fig. 4b indicated by yellow arrows), the RCM precipitation anomalies are uniformly too large compared to the observations. It is known

[1] http://www.cpc.noaa.gov/products/analysis_monitoring/ensostuff/ensoyears.ERSST.v3.shtml

that precipitation variations in the central IMW are not exactly in-phase with ENSO; instead, precipitation variations lag ENSO by a quarter-phase in both the 3-6 year frequency (Rajagopalan and Lall 1998) and the decadal frequency (Wang et al. 2009b). This feature is manifest by the weak winter precipitation anomalies in the observations near regions 3 and 4 (**Fig. 8a**), where the precipitation dipole changes sign. In the RCMs, however, significant ENSO signals remain in the central IMW extending from the Pacific Northwest, suggesting that most RCMs simulate the ENSO impacts too far inland. On the other hand, the ENSO composites made for the subsequent spring seasons (**Fig. 8b**) do not reveal such a systematic bias; this suggests that overprediction of winter precipitation over the IMW may be the cause of such a false ENSO signal.

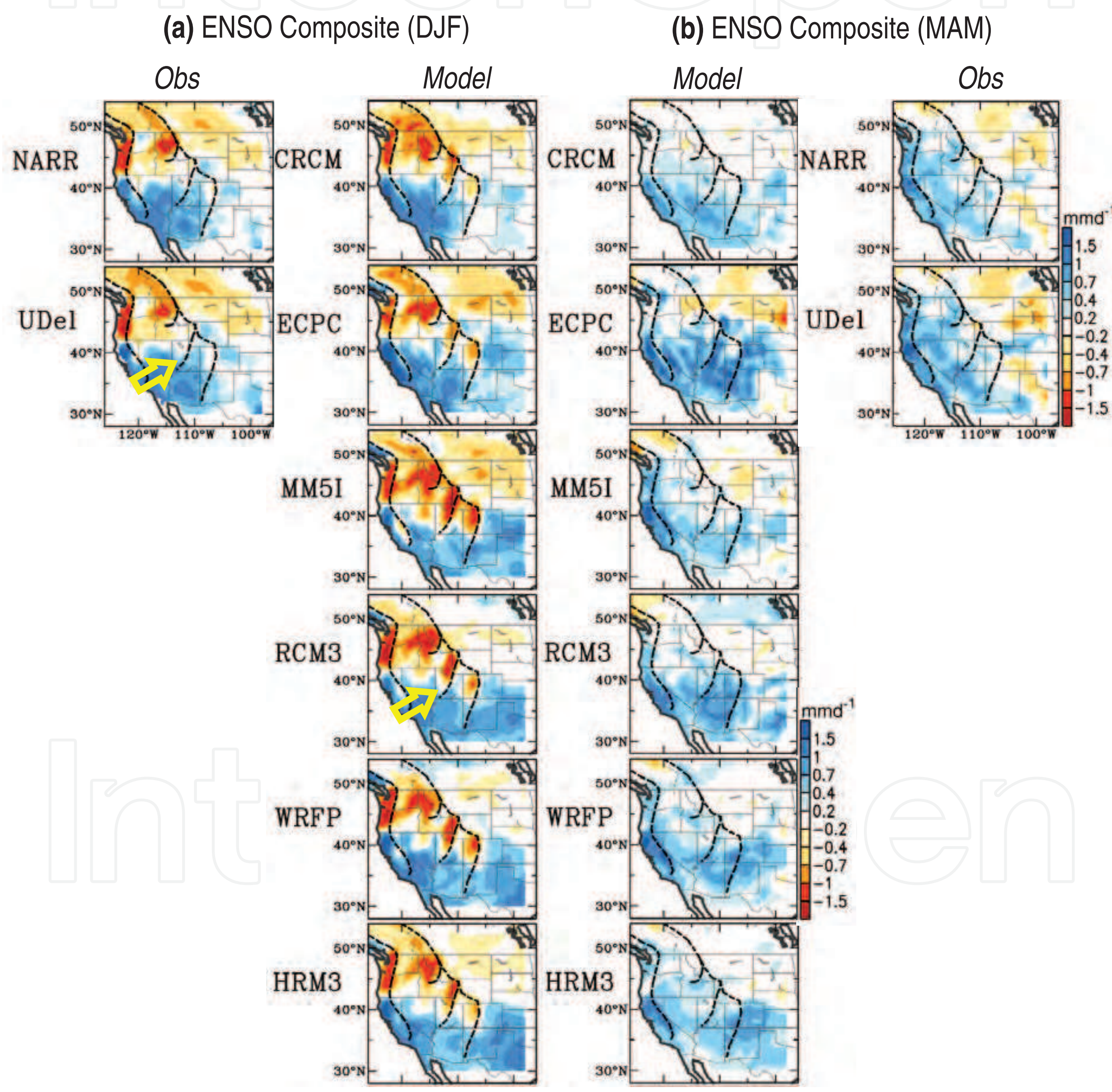

Fig. 8. (a) Differences of precipitation composites between El Niño and La Niña winters (December-February). (b) Same as (a) but for the subsequent springs (March-May). The major mountain ranges are outlined by black dashed lines. The interval of shaded contours is given in the lower right. Adopted from Wang et al. (2009a).

4. Decadal variability

a. Multi-decadal cycle

A wealth of research (Gray et al. 2003; Seager et al. 2005; Herweijer et al. 2007; and others) has established a link between low-frequency climate variability in the IMW and the Pacific climate oscillations. Recent studies focusing on the decadal-scale climate variability have turned attention to the Great Salt Lake (GSL), a large closed-basin lake located in the heart of the IMW (**Fig. 1**). As a pluvial lake, the GSL integrates hydrological forcings over a substantial watershed. When coupled with the lake's shallowness, the accumulated water results in extensive fluctuations in the lake elevation. The large drainage area of the GSL dampens out high-frequency variability and therefore is more responsive to climatic variabilities at longer timescales (Lall and Mann 1995). Consequently, the long-term change in the GSL elevation reflects the persistent wet/dry periods in the IMW. This feature is revealed in **Fig. 9a**, the GSL's 150 years of elevation record (shaded curve) superimposed with the lake elevation tendency (ΔGSL; dotted line). Applied with the 20-year lowpass filter, the ΔGSL exhibits a marked multi-decadal variability (solid line) that is coherent with the low-frequency variation of the Palmer Drought Severity Index (PDSI; red dashed line), reconstructed from tree rings near the GSL (Cook and Krusic 2004). Such a result supports the notion that any long-term changes in the GSL elevation respond to sustained wet and dry periods of the surrounding region. A recent study by Wang et al. (2011a) noticed that a multi-decadal (~30 year) and a quasi-decadal (10-15 year) frequency bands stand out significantly in the GSL elevation spectrum; this feature is shown in **Fig. 9b**. These two frequency bands are also the leading timescales of the drought variability in the IMW (Herweijer et al. 2007).

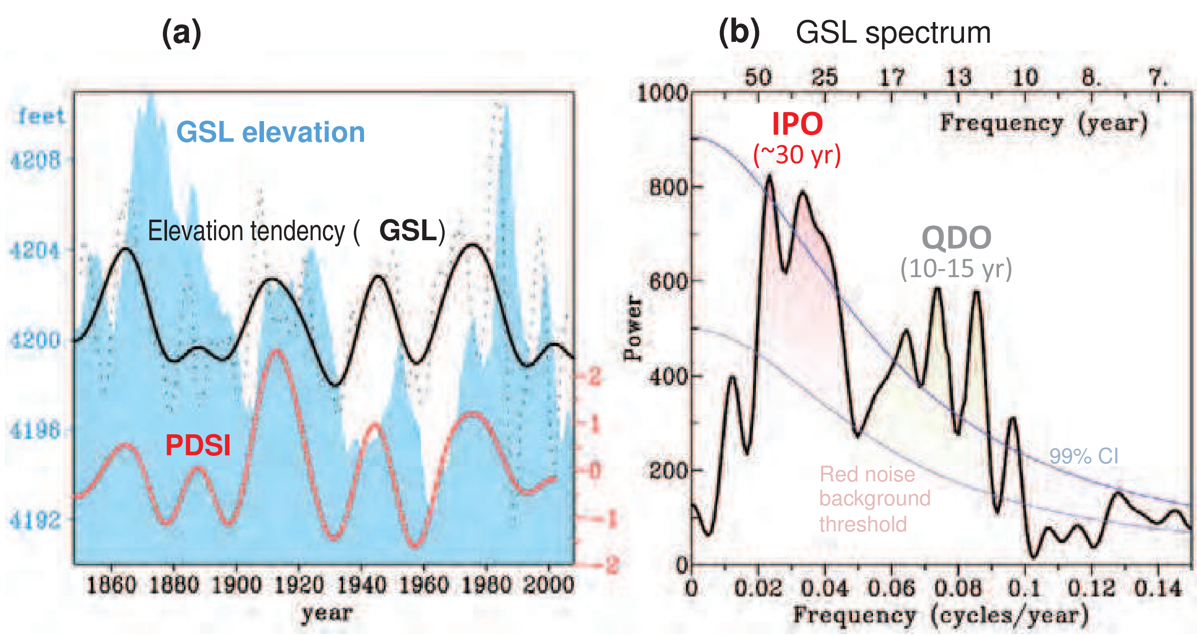

Fig. 9. (a) The GSL elevation (blue shaded graph) overlaid with the elevation tendency (ΔGSL; black line) and the PDSI (red dashed line) at the nearby grid points, after a 20-year lowpass filter. The unfiltered ΔGSL is shown with a gray dotted line for reference. (b) The Multi-Taper Method (MTM) spectral analysis of the ΔGSL during the period 1848-2008 with 2π tapper, overlaid with the 99% confidence interval (upper blue line) and the red noise background threshold (lower blue line). Adopted from Wang et al. (2011a).

The analysis of Wang et al. (2011a) revealed that hydrological factors controlling the multi-decadal variations of the GSL elevation respond to a particular teleconnection that is induced at the transition point of the IPO, that is, a basin-scale interdecadal variability that exhibits a loading pattern in the tropical Pacific SSTs (Folland et al. 2002). The transition lies approximately halfway between the warmest and coldest tropical SST anomalies in the central Pacific (corresponding to the extreme IPO phases). A distinctive teleconnection pattern develops during such transition points, as was argued by Wang et al. (2011a) and delineated in **Fig. 10**. Using a 700-year record (1300-2003) of the tree ring-reconstructed Niño 3.4 index (Cook et al. 2009), denoted as CNiño3.4, as well as the Twentieth Century Reanalysis (20CR) Version 2 during 1871-2010 (Compo et al. 2011), the 250hPa streamfunction and SSTs were regressed upon the CNiño3.4 index. All the variables were bandpass filtered with 20-45 years to reflect the IPO. At year zero (yr+0),

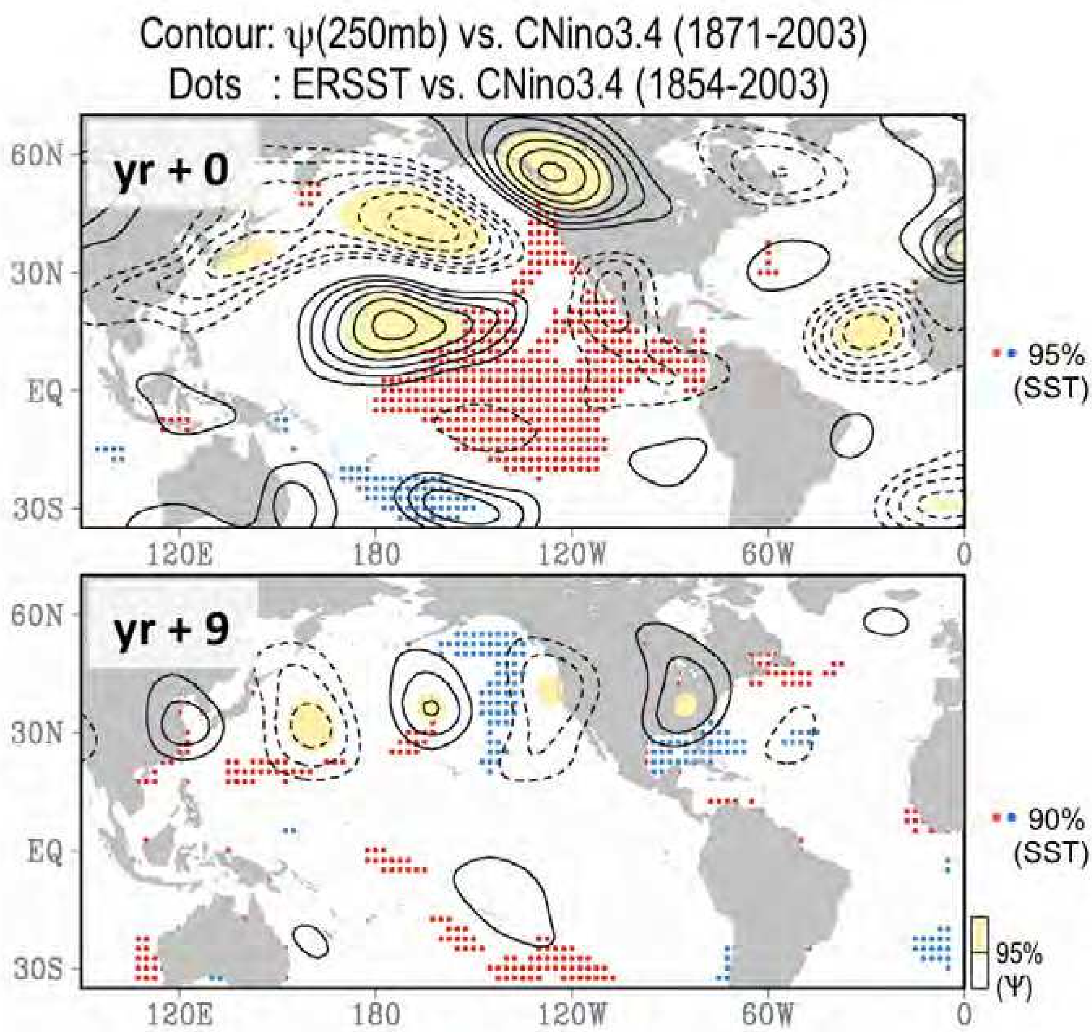

Fig. 10. (a) Patterns of the 250mb streamfunction (ψ; contours) and SSTs (dotted) regressed upon the CNiño3.4 index at different lags. The contour interval is 10-6 m2 s-1 omitting zeros. All data were bandpass filtered with 20-50 years. Values at the 95% confidence interval are indicated by yellow shadings for ψ and by dots for the SSTs, based on Student’s t-test.

the SST response to the CNiño3.4 depicts the classic IPO "horseshoe pattern" (Zhang and Delworth 2007) consisting of a widespread eastern tropical warming surrounded by midlatitude cooling. A clear PNA pattern of the streamfunction field emerges in response to such a tropical Pacific warming (**Fig. 10a**). Such SST and circulation patterns are known to produce the North American dipole that juxtaposes the GSL area with wet conditions the SST response to the CNiño3.4 depicts the classic IPO "horseshoe pattern" (Zhang and Delworth 2007) consisting of a widespread eastern tropical warming surrounded by midlatitude cooling. A clear PNA pattern of the streamfunction field emerges in response to the north and dry conditions to the south (Gershunov and Barnett 1998); however it is not the modulating force for the GSL change (Wang et al. 2009b). At yr+9, the basin-wide SST pattern reveals weak anomalies in the central equatorial Pacific with noticeable cooling in the northeastern Pacific (**Fig. 10b**). Meanwhile, a cyclonic cell develops over western North America and is embedded in a zonal wave train. Such a teleconnection wave train appears to be a Rossby wave response to upstream forcings (similar to the situation in **Fig. 7**), possibly induced by warm SST and/or convection anomalies in the western North Pacific (Lau and Weng 2002; Wang et al. 2011b). The resulting cyclonic circulation over the West Coast influences precipitation in the interior West (Barlow et al. 2001). The results presented here therefore suggest that the GSL's multi-decadal variability (and associated local wet/dry cycle) is modulated by the IPO's *transition phases* between the warm and cold, rather than by its extreme phases.

b. Quasi-decadal cycle

The marked quasi-decadal variability (10-15 year) revealed form the IMW precipitation variations, the GSL elevation change (cf. Fig. 9b), and the Pacific SSTs indicates a co-variation between the GSL elevation and the Pacific QDO. The Pacific QDO has a substantial SST variation in the central tropical Pacific near the NINO4 region (Allan 2000). At the quasi-decadal timescale, the SST anomalies in the NINO4 region [ΔSST(NINO4)] exhibit a significant, yet inverse coherence with the GSL elevation (**Fig. 11**). However, such a coherence denies any direct association (either in-phase or out-of-phase) between the precipitation anomalies in the GSL watershed and the Pacific QDO because, in a given frequency, the precipitation variations always lead the GSL elevation variations (Lall and Mann 1995). In other words, only an indirect link or a coincidence can explain such an association between the Pacific QDO and the precipitation source of the GSL.

Wang et al. (2010a) investigated this phenomenon and found that the quasi-decadal variation in the IMW precipitation consistently lags the Pacific QDO by a quarter-phase, i.e. 3 years after the peak of the warm-phase Pacific QDO occurs, an anomalous trough develops over the Gulf of Alaska and enhances the IMW precipitation (similar to the situation in **Fig. 10**). For the opposite, i.e. the cool-phase Pacific QDO, 3 years later an anomalous ridge forms in the same location and thus reduces the IMW precipitation. These findings describes a process that the quasi-decadal coherence between ΔSST(NINO4) and the GSL elevation reflects a sequential process that begins with the warm/cool phase of the Pacific QDO and ultimately affects the GSL elevation, through modulations of the quadrature amplitude modulation of the Pacific QDO. This process is illustrated in **Fig. 11** with bandpass filtered time series of ΔSST(NINO4), the IMW precipitation (P), and the GSL elevation. The phase shift creates consistent time lags between the GSL elevation and the

Pacific QDO, leading to a phase lag of ~3 years in the quasi-decadal frequency (**Fig. 11**). These processes attribute the phase lags in the occurrence of the IMW droughts/pluvials in the IMW, to the lifecycle of the decadal-scale Pacific climate oscillations.

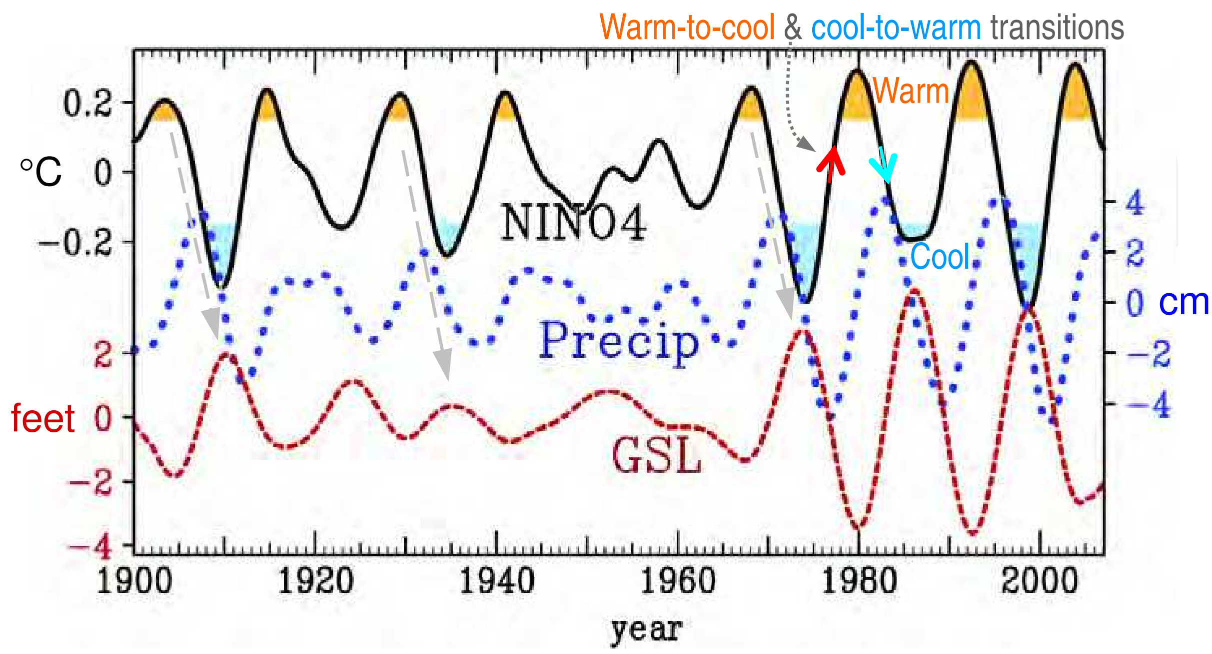

Fig. 11. Time series of the 10-15 year bandpassed ΔSST(NINO4) (black line), precipitation in the GSL watershed (blue dotted line), and the GSL elevation (red dashed line). The GSL elevation lags the precipitation by 3 years while the precipitation lags the Pacific QDO by another 3 years. (Adopted from Wang et al. 2010a) with permission of the American Meteorological Society

c. Paleoclimate evidence

Because instrumental precipitation data in the IMW only date back to the 1890s, and the length of reliable atmospheric data is considerably shorter, proxy precipitation constructed by tree-ring chronology was examined. Compiling the tree ring records in northeastern Utah, Gray et al. (2004) constructed a 776 year precipitation record from 1226 to 2001 – this data has been shown in **Fig. 1**. The power spectra of Gray et al.'s tree-ring precipitation (**Fig. 12a**) depict three significant modes, with one covering the 150-200 year frequency and the other two corresponding to the 30 year and 10-15 year cycles of the GSL elevation (cf. **Fig. 9b**). The 150-200 year mode echoes the "secular mode" of GSL that was pointed out by previous studies (Lall and Mann 1995). As shown in **Fig. 1**, its uptrend during the 20th century coincides with the climate regime shift observed in the Colorado River Basin during the 1970s (Hidalgo and Dracup 2003). The 30-year cycle of the tree-ring precipitation is most pronounced between 1500 and 1650 and has weakened since starting around 1650. Recent tree-ring chronologies have been developed into proxies for atmospheric circulation patterns. Examining the proxy index of the Pacific Decadal Oscillation (PDO) constructed by Biondi et al. (2001) for the 1661-1991 period and comparing it with Gray et al.'s tree-ring precipitation, Wang et al. (2010a) found three peaks in the 30 year, 10-15 year, and 4-5 year frequency bands that are significant above the 90% confidence level in the spectral coherence analysis (**Fig. 12b**). It is known that the PDO (which covers the North Pacific north of 20°N, in contrast to the IPO that covers the entire Pacific Basin) contains both the interdecadal and interannual signals in the tropical Pacific (Zhang et al. 1997). Therefore, the three coherence zones in **Fig. 12b** appear to be responses of the PDO, QDO, and ENSO modes, respectively. These modes not only affect the IMW climate individually but also collectively; their interplay is discussed next.

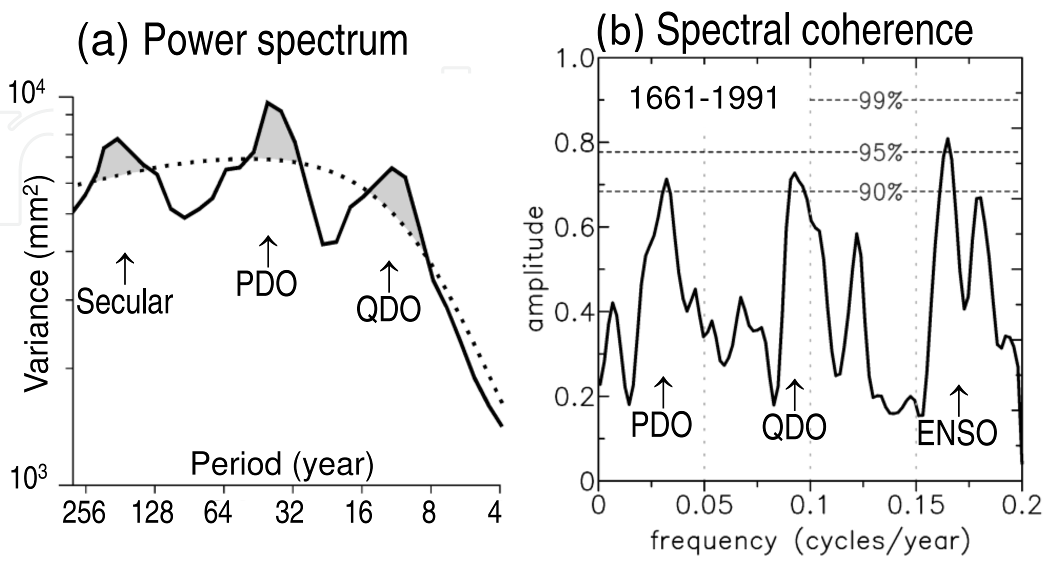

Fig. 12. (a) The global wavelet power spectrum of the tree-ring reconstructed precipitation over northeast Utah (*Gray et al. 2004*) from 1226 to 2001 superimposed with the red-noise 99% significance level (dotted curve). (b) MTM coherence between the tree-ring precipitation and the proxy PDO index constructed by Biondi et al. 2001 for 1661-1991. The three frequency bands corresponding to the IPO, QDO, and ENSO are indicated. (Adopted from Wang et al. 2010a)

5. Scale interaction between different climate modes

a. Interdecadal vs. interannual

Focusing on timescales longer than ENSO, previous studies (e.g., Gershunov and Barnett 1998; Brown and Comrie 2004) have identified a pronounced interaction between interannual and decadal climate variabilities originating from the Pacific. Those studies concluded that constructive and destructive superposition between ENSO and the PDO can respectively strengthen and weaken the North American dipole structure in precipitation and temperature. Recent studies (e.g., Brown 2011) continued to explore such a multi-decadal, ENSO-related variability over the western United States. But to date, how these different scales of natural variability interact and how such interactions influence the IMW climate remains unclear. Although ENSO is known to fluctuate within a broad frequency band of 2-7 years, several studies (e.g., Allan 2000; Tourre et al. 2001) have argued that there are two distinct modes of ENSO – a 2-3 year "quasi-biennual" oscillation and a 3-6 year interannual oscillation. These two ENSO modes are associated with unique atmosphere-ocean interactions and are linked to different regional climate patterns (Mo 2010).

To substantiate this character, time series of precipitation averaged in four western states of Nevada, Utah, Idaho and Wyoming (derived from the US Historical Climatology Network data), as well as the Nino3.4 SST index, are displayed in **Fig. 13a**. Here, both time series were bandpass filtered with 3-6 years to focus on the interannual mode, following Rajagopalan and Lall (1998). Visual inspection finds that the two variables are not consistently in-phase or out-of-phase; instead, their relationship fluctuates. By computing a running correlation analysis of every 15 years, centered at the 7th year, the relationship between the precipitation

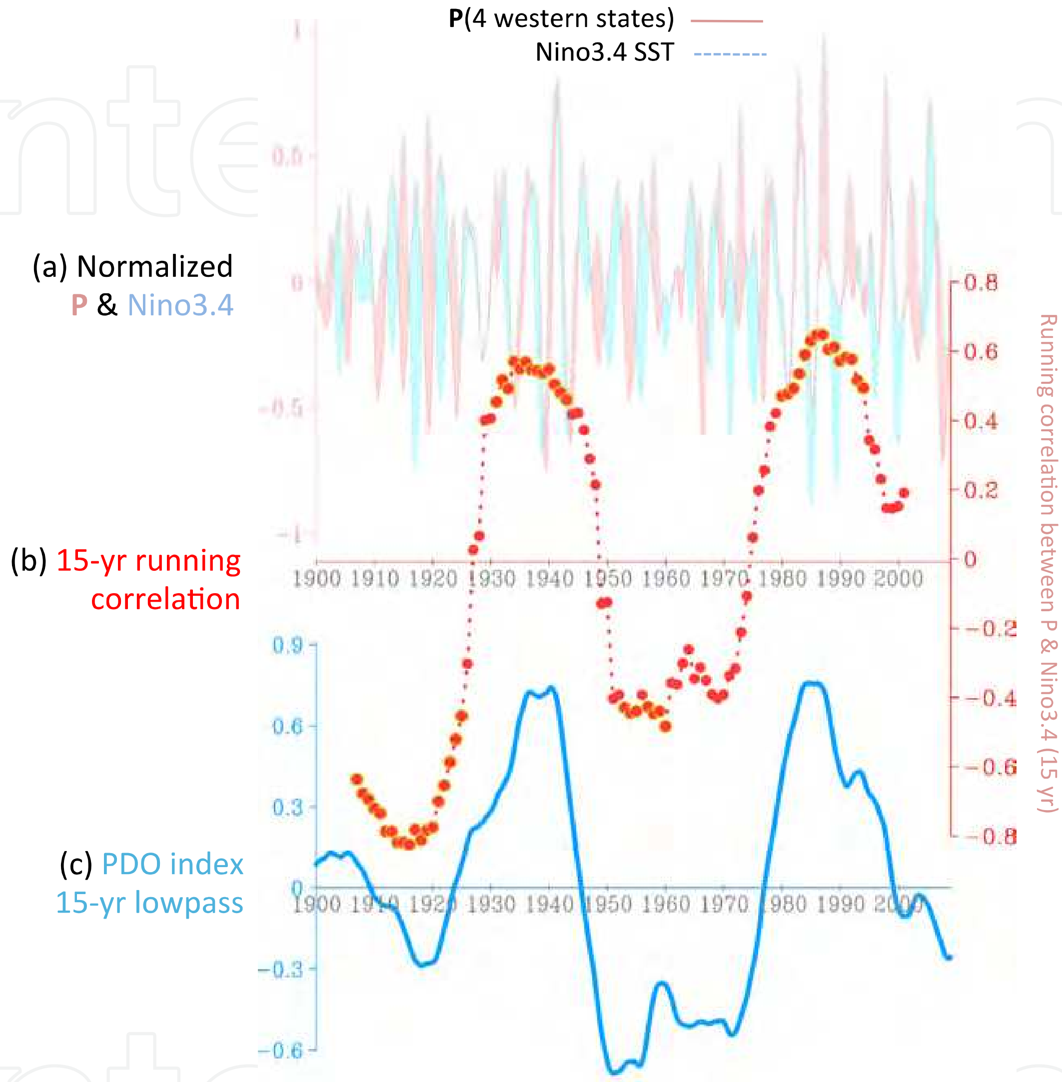

Fig. 13. (a) Time series of precipitation (P) averaged within the 4-state region (see text) and the Nino3.4 SST index. (b) Running correlation coefficients of a 15 year period between P and Nino3.4, with significant correlations outlined by yellow circles. (c) The PDO index with 15-year lowpass filter.

and Nino3.4 SST anomalies reveals a low-frequency oscillation (**Fig. 13b**), with some 20 years featuring negative correlations and the next 20 years showing positive correlations, only to transition to negative again. Superimposing the PDO index[2] smoothed by a 15-year lowpass filter (to highlight its low-frequency signal, **Fig. 13c**), it becomes clear that the alternating correlation between ENSO and the precipitation anomalies is a modulation from

[2] The PDO index was obtained from the University of Washington at http://jisao.washington.edu/pdo/PDO.latest.

the PDO. Apparently, positive PDO phases shift the ENSO-induced North American dipole northward, causing the central IMW to respond positively to ENSO. Likewise, negative PDO phases shift the dipole southward, thereby leading the central IMW to react negatively with ENSO. On the other hand, correlation analysis between the Nino3.4 SST anomalies and precipitation in Arizona and New Mexico (not shown) does not reveal any discernable change with respect to the PDO phasing. This finding result suggests that the PDO modulation on ENSO's climate impact is only effective around the transition zone of the precipitation dipole in the central IMW. This result echoes the observation by Brown (2011) that the relationship between cold-season ENSO conditions and circulation anomalies over the western United States varies with phasing of the PDO. The results presented here and from Brown (2011) therefore suggest uncertainty on decadal time scales for using ENSO conditions as a seasonal climate forecast tool.

b. Interannual vs. intraseasonal

We have observed that the intraseasonal variability of the IMW climate also undergoes modulation from certain interannual modes. Analyzing episodes of persistent temperature inversions in Salt Lake Valley and Cache Valley (80 miles northeast of Salt Lake City), Gillies et al. (2010a) noticed a tendency for those persistent inversion episodes to delay their occurrence by about 5 days each year. This intriguing feature is illustrated in **Fig. 14a,** which

shows the temperature lapse rate at the Salt Lake City International Airport (KSLC; shadings) overlaid with the PM2.5 concentrations in Salt Lake City (blue line), for winters 1998/99 to 2007/08. Throughout this decade, the occurrences of persistent temperature inversions (i.e. events lasting longer than 7 days) began in mid-December 1998, shifted to late December in 1999 and then continued to "delay" through late January 2007. Because such prolonged temperature inversion events are linked to episodes of semi-stationary ridge developed over the IMW, we analyzed the NCEP/NCAR Reanalysis (Kalnay et al. 1996) using the 700hPa geopotential height at the nearest grid point of KSLC from December 1948 to February 2010. The geopotential height was bandpass filtered with 20-40 days based on the 30-day mode as identified in Gillies et al. (2010a). The analysis of 62 winters (**Fig. 14b**) reveals episodes of prolonged ridge events (dark gray) that seem to delay each year by one week, as indicated by yellow arrows. This "migration" in the timing of the ridging episodes reappears in early December about every 5-6 years. This timescale coincides with that of the interannual ENSO cycle. It is possible that persistent ridging and inversion episodes in the IMW undergo an external forcing that modulates the seasonal timing of their occurrence.

To examine the possible interannual forcing on the intraseasonal variability of the persistent ridging events principal component (PC) analysis was carried out using the bandpass filtered 700hPa geopotential height as that shown in Fig. 14b. The first two leading modes (PC1 and PC2; **Fig. 15a**), accounting for 27% and 19% of the variance, depict a quadrature phase shift in the timing of the intraseasonal fluctuation. The year-to-year coefficients of PC1 and PC2 are significantly correlated at a 1-year lag (r=0.48), suggesting that PC1 tends to transitions into PC2 a year after. Meanwhile, PC3 shows weaker amplitude in the middle of the winter (9% of the variance). The regression patterns of winter streamfunction at 300 hPa and SSTs with each PC coefficient are shown in **Fig. 15b**. The regression with PC1 reveals a La Nina type of SST and circulation structure characterized by cold SST anomalies in the central equatorial Pacific associated with a PNA-like teleconnection pattern. The regression with PC2 depicts weak and disorganized SST anomalies accompanied by a short-wave circulation pattern. Noteworthy is that this short-wave pattern is in-phase with the winter standing wave train, similar to that presented in Fig. 7a, but at a slightly different latitude with respect to the winter jet stream. The troughs (red) and ridges (blue) of the winter standing wave train are indicated in **Fig. 15b**. Likely, PC2 is at the transition point between the La Nina and El Nino phases, where short-wave circulation response is a dominant feature (Wang et al. 2011b). The regression with PC3 outlines the SST and circulation patterns very similar to the North Atlantic Oscillation (Hurrell 2003), with a seesawing dipole between the Icelandic low and the Bermuda high. This mode (PC3) appears to modify the transition between PC1 and PC2 and further change the occurrence timing. These observations require further examination through GCM experiments prescribed with SST forcing conditions as those in **Fig. 15**.

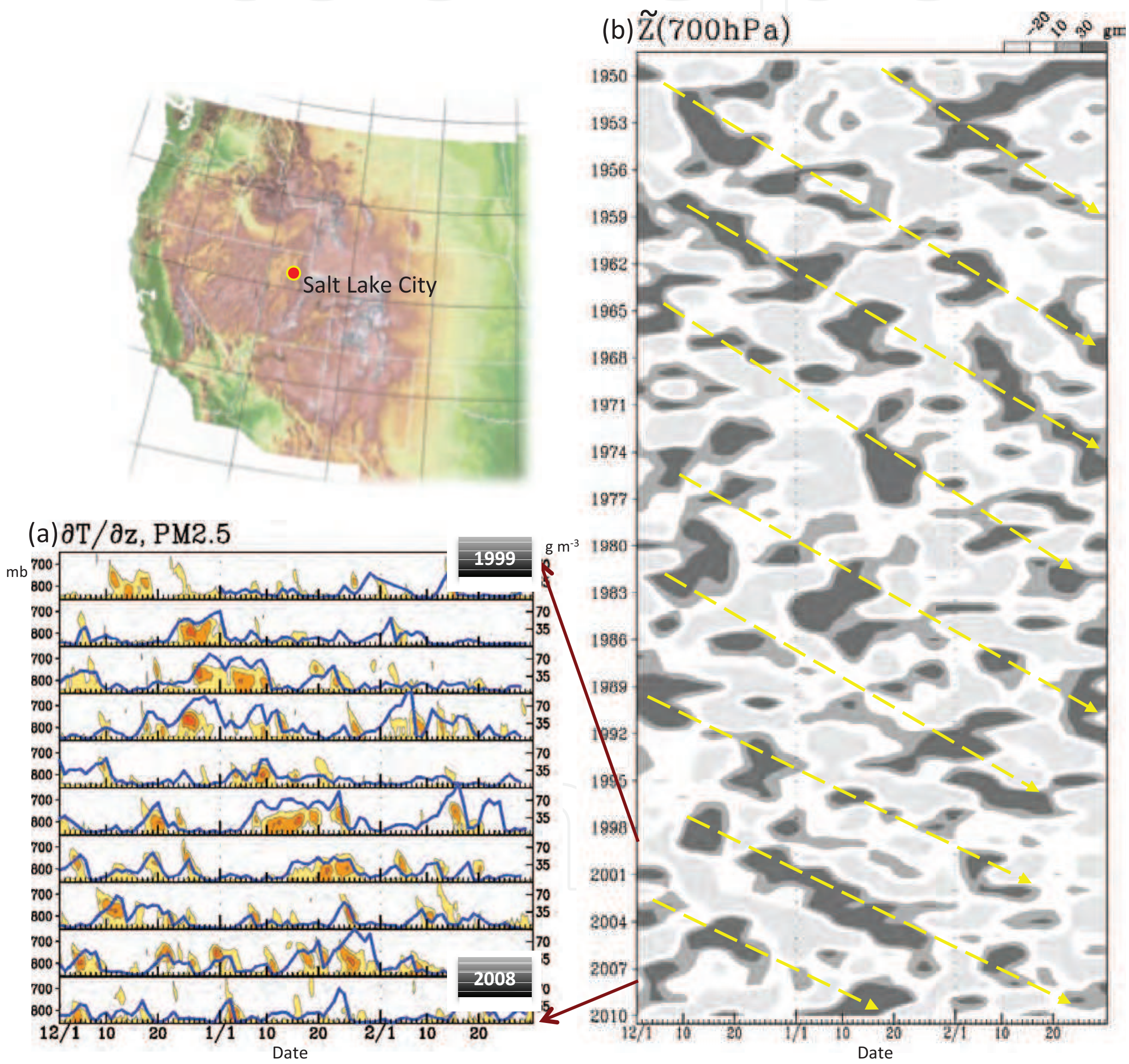

Fig. 14. (a) The 00Z temperature lapse rate at KSLC (orange contours) overlaid with PM2.5 concentrations within Salt Lake Valley for the winters of 1999-2008. (b) Bandpass filtered geopotential height at 700mb with 20-40 days interpolated onto the KSLC location derived from NCEP reanalysis; yellow arrows indicate the time shift in persistent ridging events. The geographical location and terrain are given at top left.

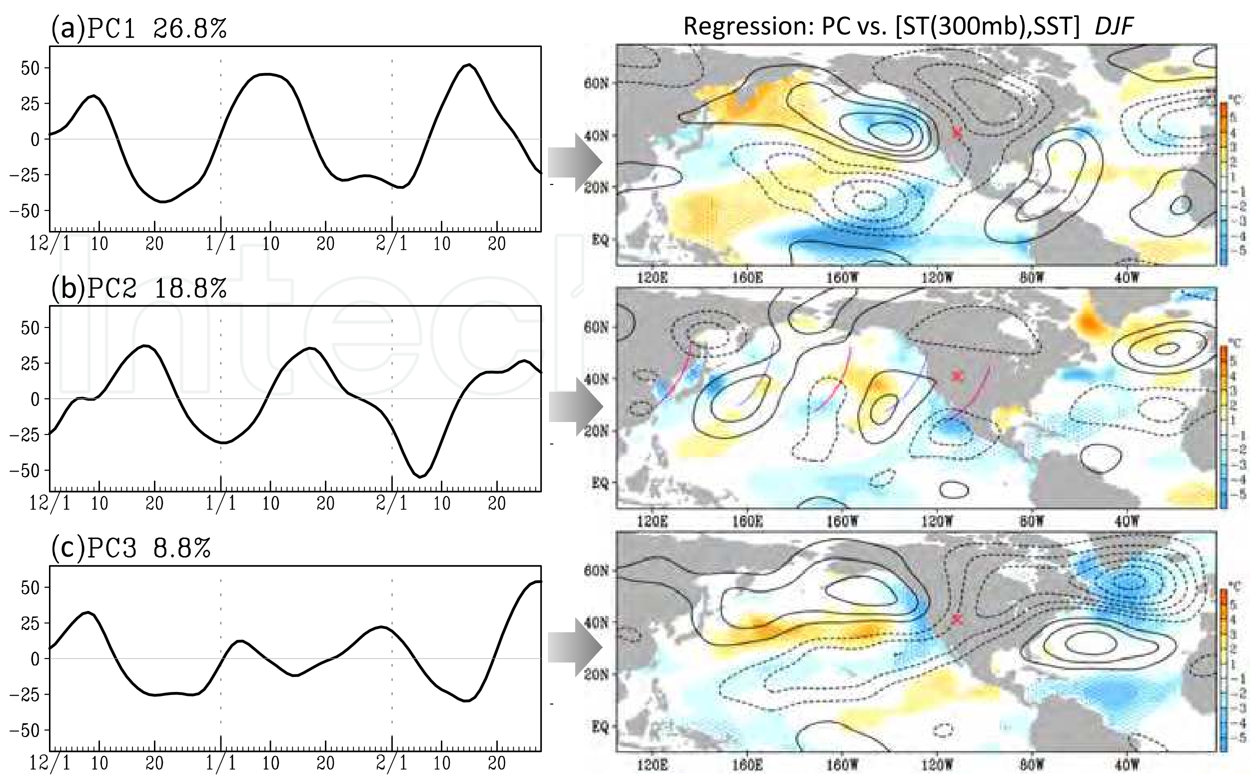

Fig. 15. (a) First 3 leading PCs of the bandpass filtered 700mb geopotential height at KSLC over the 1980-2008 period, and (b) corresponding patterns of 300mb streamfunction (contours) and SSTs (shading) regressed upon each PC time series. KSLC is indicated by a red cross.

6. Summary

The IMW is situated in the marginal zone of different climate regimes between (a) the annual and semiannual cycles, (b) the ENSO-induced north-south dipole, and (c) the PDO-related north-south seesaw pattern. The IMW climate variability undergoes robust modulations by the Pacific teleconnection. However, past research has almost exclusively focused on the extreme phases of the Pacific oscillatory modes (such as ENSO and the PDO/IPO), even though those modes feature a well-defined lifecycle. In this chapter we demonstrated that the Pacific oscillatory modes induce different types of teleconnection during their transition between the extreme warm and cold phases. Such teleconnection processes are subtle and may be difficult to monitor, but they have been found to control the climate variability of the IMW more profoundly than the warm/cold phases of the Pacific oscillatory modes. Moreover, the circulation anomalies affecting the IMW are more responsive to midlatitude short-wave trains rather than the long-wave PNA pattern. This feature poses a challenge to climate modeling and seasonal climate prediction for the IMW, especially the upper Colorado River Basin. The interplay between the various climate oscillations and their collective effects further complicate the climate variability of the IMW. Current climate forecast models have a difficulty in realistically depicting the IMW's climate regime and the transition-phase teleconnections associated with ENSO (and /IPO).

In the changing climate, future water resources of the IMW may be strained and threatened due to the rapid increase in water demand and the projected decrease in precipitation.

Historical climate data indicate that episodic events of extreme drought will compound the problem of increased demand and that this may interact with projected climate change in unforeseen and potentially worrisome ways. This is particularly a concern for water management in the IMW, which supplies the headwater of the Colorado River. Further diagnostics and modeling studies are required to isolate the effect of individual climate oscillatory modes in order to improve climate prediction for the IMW.

7. Acknowledgements

We are indebted to Dr. Xiaoqing Wu at Iowa State University for sharing the CCM3 simulation data. Insightful comments from Dr. Huug van dan Dool of the Climate Prediction Center are highly appreciated. This study was supported by the Utah State University Agricultural Experiment Station and approved as paper number 8359, as well as the Bureau of Reclamation Grant R11AC81456.

8. References

Allan, R., 2000: ENSO and climatic variability in the last 150 years. *El Niño and the Southern Oscillation: Multiscale Variability, Global and Regional Impacts*, H. F. Diaz, and V. Markgrav, Eds., Cambridge Univ. Press, 3–56.

Barlow, M., S. Nigam, and E. H. Berbery, 2001: ENSO, Pacific Decadal Variability, and U.S. Summertime Precipitation, Drought, and Stream Flow. *J. Climate*, 14, 2105-2128.

Barnett, T. P., and D. W. Pierce, 2008: When will Lake Mead go dry? *Water Resour. Res.*, 44, W03201.

Biondi, F., A. Gershunov, and D. R. Cayan, 2001: North Pacific Decadal Climate Variability since 1661. *J. Climate*, 14, 5-10.

Boyle, J. S., 1998: Evaluation of the Annual Cycle of Precipitation over the United States in GCMs: AMIP Simulations. *J. Climate*, 11, 1041-1055.

Branstator, G., 1987: A Striking Example of the Atmosphere's Leading Traveling Pattern. *J. Atmos. Sci.*, 44, 2310-2323.

— —, 2002: Circumglobal Teleconnections, the Jet Stream Waveguide, and the North Atlantic Oscillation. *J. Climate*, 15, 1893-1910.

Brown, D. P., 2011: Winter Circulation Anomalies in the Western United States Associated with Antecedent and Decadal ENSO Variability. *Earth Interactions*, 15, 1-12.

Brown, D. P., and A. C. Comrie, 2004: A winter precipitation "dipole" in the western United States associated with multidecadal ENSO variability. *Geophys. Res. Lett.*, 31, L09203.

Compo, G. P., and Coauthors, 2011: The Twentieth Century Reanalysis Project. *Q. J. Roy. Meteor. Soc.*, 137, 1-28.

Cook, E. R., and P. J. Krusic, 2004: North American summer PDSI reconstructions, 24 pp.

Cook, E. R., D. M. Meko, and C. W. Stockton, 1997: A New Assessment of Possible Solar and Lunar Forcing of the Bidecadal Drought Rhythm in the Western United States. *J. Climate*, 10, 1343-1356.

Cook, E. R., R. D. D'Arrigo, and K. J. Anchukaitis, 2009: Tree Ring 500 Year ENSO Index Reconstructions# 2009-105.

Dettinger, M. D., D. R. Cayan, H. F. Diaz, and D. M. Meko, 1998: North–South Precipitation Patterns in Western North America on Interannual-to-Decadal Timescales. *J. Climate*, 11, 3095-3111.

Ding, Q., and B. Wang, 2005: Circumglobal Teleconnection in the Northern Hemisphere Summer*. *J. Climate*, 18, 3483-3505.

Folland, C. K., J. A. Renwick, M. J. Salinger, and A. B. Mullan, 2002: Relative influences of the Interdecadal Pacific Oscillation and ENSO on the South Pacific Convergence Zone. *Geophys. Res. Lett.*, 29, 1643.

Gershunov, A., and T. P. Barnett, 1998: Interdecadal Modulation of ENSO Teleconnections. *Bull. Amer. Meteor. Soc.*, 79, 2715-2725.

Gillies, R. R., S.-Y. Wang, and M. R. Booth, 2010a: Atmospheric scale interactions on wintertime Intermountain West inversions. *Wea. Forecasting*, 25, 1196–1210.

Gillies, R. R., S.-Y. Wang, J.-H. Yoon, and S. Weaver, 2010b: CFS Prediction of Winter Persistent Inversions in the Intermountain Region. *Wea. Forecasting*, 25, 1211–1218.

Gray, S. T., S. T. Jackson, and J. L. Betancourt, 2004: Tree-ring based reconstructions of interannual to decadal-scale precipitation variability for northeastern Utah. *J. Amer. Water Resour. Assoc*, 40, 947–960.

Gray, S. T., J. L. Betancourt, C. L. Fastie, and S. T. Jackson, 2003: Patterns and sources of multidecadal oscillations in drought-sensitive tree-ring records from the central and southern Rocky Mountains. *Geophys. Res. Lett.*, 30, 49-41 - 49-44.

Herweijer, C., R. Seager, E. R. Cook, and J. Emile-Geay, 2007: North American Droughts of the Last Millennium from a Gridded Network of Tree-Ring Data. *J. Climate*, 20, 1353-1376.

Hidalgo, H. G., and J. A. Dracup, 2003: ENSO and PDO Effects on Hydroclimatic Variations of the Upper Colorado River Basin. *Journal of Hydrometeorology*, 4, 5-23.

Higgins, R. W., Y. Yao, and X. L. Wang, 1997: Influence of the North American Monsoon System on the U.S. Summer Precipitation Regime. *J. Climate*, 10, 2600-2622.

Horel, J. D., and J. M. Wallace, 1981: Planetary-Scale Atmospheric Phenomena Associated with the Southern Oscillation. *Mon. Wea. Rev.*, 109, 813-829.

Horel, J. D., and C. R. Mechoso, 1988: Observed and Simulated Intraseasonal Variability of the Wintertime Planetary Circulation. *J. Climate*, 1, 582-599.

Hoskins, B. J., and D. J. Karoly, 1981: The Steady Linear Response of a Spherical Atmosphere to Thermal and Orographic Forcing. *J. Atmos. Sci.*, 38, 1179-1196.

Hsu, C.-P. F., and J. M. Wallace, 1976: The Global Distribution of the Annual and Semiannual Cycles in Precipitation. *Mon. Wea. Rev.*, 104, 1093-1101.

Hurrell, J. W., 2003: *The North Atlantic oscillation: climatic significance and environmental impact.* Vol. 134, American Geophysical Union, 279 pp.

Kalnay, E., and Coauthors, 1996: The NCEP/NCAR 40-Year Reanalysis Project. *Bull. Amer. Meteor. Soc.*, 77, 437-471.

Kushnir, Y., 1987: Retrograding Wintertime Low-Frequency Disturbances over the North Pacific Ocean. *J. Atmos. Sci.*, 44, 2727-2742.

Lall, U., and M. E. Mann, 1995: The Great Salt Lake: A barometer of low-frequency climatic variability. *Water Resour. Res.*, 31, 2503-2515.

Lau, K. M., and H. Weng, 2002: Recurrent Teleconnection Patterns Linking Summertime Precipitation Variability over East Asia and North America. *Journal of the Meteorological Society of Japan*, 80, 1309-1324.

Lau, N.-C., and M. J. Nath, 1999: Observed and GCM-Simulated Westward-Propagating, Planetary-Scale Fluctuations with Approximately Three-Week Periods. *Mon. Wea. Rev.*, 127, 2324-2345.

Legates, D. R., and C. J. Willmott, 1990: Mean seasonal and spatial variability in gauge-corrected, global precipitation. *Int. J. Climatol.*, 10, 111-127.

Leung, L. R., Y.H. Kuo, and J. Tribbia, 2006: Research needs and directions of regional climate modeling using WRF and CCSM. *Bull. Amer. Meteor. Soc.*, 87, 1747–1751.

Mantua, N. J., S. R. Hare, Y. Zhang, J. M. Wallace, and R. C. Francis, 1997: A Pacific Interdecadal Climate Oscillation with Impacts on Salmon Production. *Bull. Amer. Meteor. Soc.*, 78, 1069-1079.

Marks, D., and A. Winstral, 2001: Comparison of Snow Deposition, the Snow Cover Energy Balance, and Snowmelt at Two Sites in a Semiarid Mountain Basin. *Journal of Hydrometeorology*, 2, 213-227.

Mearns, L., W. J. J. Gutowski, R. Jones, R. Leung, S. McGinnis, A. Nunes, and Y. Qian, 2009: A Regional Climate Change Assessment Program for North America. *Eos Trans. AGU*, 90, 311-312.

Mesinger, F., and Coauthors, 2006: North American Regional Reanalysis. *Bull. Amer. Meteor. Soc.*, 87, 343-360.

Mo, K., and J. Paegle, 2005: Pan-America. *Intraseasonal variability in the atmosphere-ocean climate system*, K.-M. L. a. D. E. Waliser, Ed., Springer, 95-124.

Mo, K. C., 1999: Alternating Wet and Dry Episodes over California and Intraseasonal Oscillations. *Mon. Wea. Rev.*, 127, 2759-2776.

——, 2010: Interdecadal Modulation of the Impact of ENSO on Precipitation and Temperature over the United States. *J. Climate*, 23, 3639-3656.

Moncrieff, M. W., 1992: Organized Convective Systems: Archetypal Dynamical Models, Mass and Momentum Flux Theory, and Parametrization. *Quarterly Journal of the Royal Meteorological Society*, 118, 819-850.

Rajagopalan, B., and U. Lall, 1998: Interannual variability in western US precipitation. *Journal of Hydrology*, 210, 51-67.

Sangoyomi, T. B., 1993: Climatic variability and dynamics of Great Salt Lake hydrology, PhD, Utah State University, 247 pp.

Schubert, S., and Coauthors, 2009: A U.S. CLIVAR Project to Assess and Compare the Responses of Global Climate Models to Drought-Related SST Forcing Patterns: Overview and Results. *J. Climate*, 22, 5251-5272.

Schubert, S. D., M. J. Suarez, P. J. Pegion, R. D. Koster, and J. T. Bacmeister, 2004: On the Cause of the 1930s Dust Bowl. *Science*, 303, 1855-1859.

Seager, R., Y. Kushnir, C. Herweijer, N. Naik, and J. Velez, 2005: Modeling of Tropical Forcing of Persistent Droughts and Pluvials over Western North America: 1856–2000*. *J. Climate*, 18, 4065-4088.

Simmons, A. S., D. D. Uppala, and S. Kobayashi, 2007: ERA-interim: new ECMWF reanalysis products from 1989 onwards. *CMWF Newsl* 110, 29-35.

Tourre, Y., B. Rajagopalan, Y. Kushnir, M. Barlow, and W. White, 2001: Patterns of Coherent Decadal and Interdecadal Climate Signals in the Pacific Basin During the 20 th Century. *Geophys. Res. Lett.*, 28, 2069-2072.

Wang, S.-Y., and T.-C. Chen, 2009: The Late-Spring Maximum of Rainfall over the U.S. Central Plains and the Role of the Low-Level Jet. *J. Climate*, 22, 4696-4709.

Wang, S.-Y., R. R. Gillies, and T. Reichler, 2011a: Multi-decadal drought cycles in the Great Basin recorded by the Great Salt Lake: Modulation from a transition-phase teleconnection. *J. Climate*. doi: http://dx.doi.org/10.1175/2011JCLI4225.1

Wang, S.-Y., R. R. Gillies, E. S. Takle, and W. J. Gutowski Jr., 2009a: Evaluation of precipitation in the Intermountain Region as simulated by the NARCCAP regional climate models. *Geophys. Res. Lett.*, 36, L11704.

Wang, S.-Y., R. R. Gillies, J. Jin, and L. E. Hipps, 2009b: Recent rainfall cycle in the Intermountain Region as a quadrature amplitude modulation from the Pacific decadal oscillation. *Geophys. Res. Lett.*, 36, L02705.

Wang, S.-Y., R. R. Gillies, J. Jin, and L. E. Hipps, 2010a: Coherence between the Great Salt Lake Level and the Pacific Quasi-Decadal Oscillation. *J. Climate*, 23, 2161-2177.

Wang, S.-Y., R. R. Gillies, L. E. Hipps, and J. Jin, 2011b: A transition-phase teleconnection of the Pacific quasi-decadal oscillation. *Clim. Dynamics*, 36, 681-693.

Wang, S.-Y., L. E. Hipps, R. R. Gillies, X. Jiang, and A. L. Moller, 2010b: Circumglobal teleconnection and early summer rainfall in the US Intermountain West. *Theor. Appl. Climatol.*, 102, 245-252.

White, W. B., and Z. Liu, 2008: Resonant excitation of the quasi-decadal oscillation by the 11-year signal in the Sun's irradiance. *J. Geophys. Res.*, 113, 1-16.

White, W. B., Y. M. Tourre, M. Barlow, and M. Dettinger, 2003: A delayed action oscillator shared by biennial, interannual, and decadal signals in the Pacific Basin. *J. Geophys. Res.*, 108, 15-11 - 15-18.

Wood, A. W., 2011: Development of a Seasonal Climate and Stream Flow Forecasting Test Bed for the Colorado River Basin. *36th Climate Diagnostic and Prediction Workshop*.

Wu, X., L. Deng, X. Song, and G. J. Zhang, 2007: Coupling of Convective Momentum Transport with Convective Heating in Global Climate Simulations. *J. Atmos. Sci.*, 64, 1334-1349.

Xie, P., and P. A. Arkin, 1997: Global Precipitation: A 17-Year Monthly Analysis Based on Gauge Observations, Satellite Estimates, and Numerical Model Outputs. *Bull. Amer. Meteor. Soc.*, 78, 2539-2558.

Zhang, R., and T. L. Delworth, 2007: Impact of the Atlantic Multidecadal Oscillation on North Pacific climate variability. *Geophys. Res. Lett.*, 34, L23708.

Zhang, Y., J. M. Wallace, and D. S. Battisti, 1997: ENSO-like Interdecadal Variability: 1900–93. *J. Climate*, 10, 1004-1020.

Zhang, Z., and M. E. Mann, 2005: Coupled patterns of spatiotemporal variability in Northern Hemisphere sea level pressure and conterminous U.S. drought. *J. Geophy. Res.*, 110, D03108.

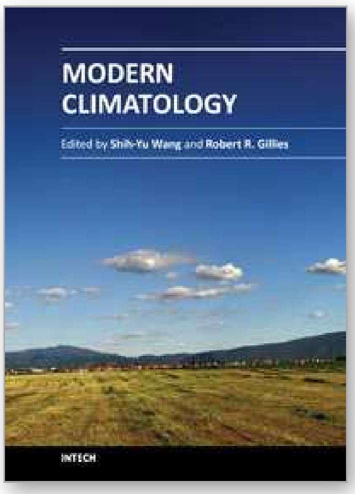

Modern Climatology

Edited by Dr Shih-Yu Wang

ISBN 978-953-51-0095-9
Hard cover, 398 pages
Publisher InTech
Published online 09, March, 2012
Published in print edition March, 2012

Climatology, the study of climate, is no longer regarded as a single discipline that treats climate as something that fluctuates only within the unchanging boundaries described by historical statistics. The field has recognized that climate is something that changes continually under the influence of physical and biological forces and so, cannot be understood in isolation but rather, is one that includes diverse scientific disciplines that play their role in understanding a highly complex coupled "whole system" that is the earth's climate. The modern era of climatology is echoed in this book. On the one hand it offers a broad synoptic perspective but also considers the regional standpoint, as it is this that affects what people need from climatology. Aspects on the topic of climate change - what is often considered a contradiction in terms - is also addressed. It is all too evident these days that what recent work in climatology has revealed carries profound implications for economic and social policy; it is with these in mind that the final chapters consider acumens as to the application of what has been learned to date.

INTECH
open science | open minds

InTech Europe
University Campus STeP Ri
Slavka Krautzeka 83/A
51000 Rijeka, Croatia
Phone: +385 (51) 770 447
Fax: +385 (51) 686 166
www.intechopen.com

InTech China
Unit 405, Office Block, Hotel Equatorial Shanghai
No.65, Yan An Road (West), Shanghai, 200040, China
中国上海市延安西路65号上海国际贵都大饭店办公楼405单元
Phone: +86-21-62489820
Fax: +86-21-62489821